NASA Technical Memorandum 100968

Particle Sizing by Weighted Measurements of Scattered Light

Donald R. Buchele
Lewis Research Center
Cleveland, Ohio

October 1988

NASA

PARTICLE SIZING BY WEIGHTED MEASUREMENTS OF SCATTERED LIGHT

Donald R. Buchele
National Aeronautics and Space Administration
Lewis Research Center
Cleveland, Ohio 44135

SUMMARY

A description is given of a measurement method, applicable to a polydispersion of particles, in which the intensity of scattered light at any angle is weighted by a factor proportional to that angle. Determination is then made of four angles at which the weighted intensity is four fractions of the maximum intensity. These yield four characteristic diameters: the diameters of the volume/area mean (D_{32} the Sauter mean) and the volume/diameter mean (D_{31}); the diameters at cumulative volume fractions of 0.5 ($D_{V0.5}$ the volume median) and 0.75 ($D_{V0.75}$). They also yield the volume dispersion of diameters. Mie scatter computations show that an average diameter less than three micrometers cannot be accurately measured. The results are relatively insensitive to extraneous background light and to the nature of the diameter distribution. Also described is an experimental method of verifying the conclusions by using two microscope slides coated with polystyrene microspheres to simulate the particles and the background.

E-4396

INTRODUCTION

This paper deals with the problem of determining by optical methods (a) the mean diameter of a large aggregate of particles such as occurs in fuel atomization studies or in aircraft icing studies and (b) a measure of the dispersion of particle diameters. The particles are produced by atomization of a continuously flowing liquid. The number of particles in the field of view is usually greater than 100.

When the particle diameter is greater than the wavelength of radiation, the diameter can be inferred from the angular distribution of light scattered in the forward direction from a collimated beam.

Reference 1 shows that a useful measure of particle diameter is derivable from the shape of the center lobe of the intensity distribution of forward-scattered radiation. The intensity may be calculated by the Fraunhofer diffraction formula instead of the more exact Mie formula. Although there is a substantial discrepancy between the two formulas in the calculation of absolute intensity when the particle diameter approaches the wavelength of the radiation, the absolute value of intensity can be eliminated by measuring the ratio of intensities at two fixed scattering angles. The lower limit of measurable particle diameter then becomes of the order of the wavelength of the radiation. The upper limit of measurable particle diameter is set by the increasing difficulty of measuring intensities as the angular width of the center lobe becomes smaller for a larger particle diameter. When measuring particles larger than 10 μm in diameter, the intensity in the center lobe is due principally to Fraunhofer diffraction rather than to the additional processes of reflection, refraction, and absorption that are included in Mie's analysis.

Reference 2, an application of reference 1, measured the angles, one fixed and one variable, where there exists a fixed ratio of two intensities. The methods of references 1 and 2 were compared by reference 3. However, both methods are limited in accuracy by extraneous background light. The method presented here enables the two angles of measurement to be chosen in such manner as to reduce the effect of extraneous light. This method is similar to that used by references 4 and 5 to determine particle diameter distribution, except that in those references, the effect of extraneous light was not considered; more recently, the effect of extraneous light was treated by references 3 and 6, and it is treated in detail in this report.

When there is a polydispersion of particles, it is generally recognized that the Sauter mean diameter (D_{32}) is a good parameter to use in studying fuel combustion rates, and the volume median diameter ($D_{V0.5}$) is a good parameter to use in studying icing conditions for aircraft in clouds and rain. The polydispersion may be characterized by its dispersion (the span of particle diameters) and by its shape as given by the analytic form of the distribution function. References 7 and 8 show that the light-scatter curve determines D_{32} nearly independently of the particle diameter distribution function.In the present work, this independence is confirmed for a narrow range of dispersions, but, contrary to references 7 and 8, there is found to be a strong dependence on the dispersion of particle sizes. To minimize this dependence, we find a point on the scattered-light intensity curve at which the intensity is a specified fraction of the maximum intensity. Four intensity ratios are chosen so that the diameters D_{32}, D_{31}, $D_{V0.5}$ and $D_{V0.75}$ are determined, and these values are substantially independent of both the distribution function and its dispersion. Furthermore, the dispersion is also determined by these measurements. The ratio $D_{V0.75}/D_{V0.5}$ may be useful as a measure of the relative amount of large diameter particles. This ratio has served to indicate the transition through a bimodal volume distribution as air assist in a spray nozzle was increased from zero. The ratio D_{31}/D_{32} may be useful to better characterize the spray when there is evaporation.

This paper also describes a means of simulating the actual physical situation by an optical-laboratory experiment. Commercially available microspheres are deposited on glass plates to simulate both a spray of droplets and the extraneous background light that interferes with the measurement. The methods of properly correcting for this background are presented and experimentally confirmed.

TERMINOLOGY

Symbols used in this paper are presented in Appendix A. A further definition of some terms will be given here.

Ordinarily, a large aggregate of liquid droplets will consist of droplets of varying diameter D, ranging from a minimum value D_ℓ to a maximum value D_u. In any given volume V_o, the number of particles whose diameters lie in a certain narrow range of diameters is conveniently represented by a number distribution function

$$dn/dD$$

where dn denotes the number fraction of particles lying in the diameter range dD and

$$\int_{D_\ell}^{D_u} (dn/dD)\,dD = 1$$

Similarly, one may define a volume distribution function

$$dV/dD$$

where dV represents the total volume of all particles lying in the diameter range dD and

$$\int_{D_\ell}^{D_u} (dV/dD)\,dD = V_o$$

For reasons of mathematical convenience or of convenience in physical analysis, the lower limit may, on occasion, be taken either as zero or as a small multiple of the wavelength of light being used. For the same reasons, the upper limit D_u may be taken as infinity or as some arbitrary finite value.

The aggregate of particles may often be characterized by (a) a single central value of diameter and (b) a single parameter that represents the dispersion of diameters about that central value. In fuel combustion studies, the most useful central value has been found to be the Sauter mean diameter D_{32} given by

$$D_{32} = \int_{D_\ell}^{D_u} (dn/dD) \cdot D^3 dD \Big/ \int_{D_\ell}^{D_u} (dn/dD) \cdot D^2 dD$$

In aircraft icing research, the most useful central value has been found to be the volume median diameter $D_{v0.5}$ given by

$$V_o/2 = \int_{D_\ell}^{D_{v0.5}} (dV/dD)\,dD$$

The terminology used here follows that of ASTM Standard Practice E799-81, reference 9, which may be consulted for more detail.

THE SCANNING-SLIT METHOD

Mechanical Arrangement

An optical system described in references 7 and 10 for measuring the radiant flux at any small angle of forward scattering is shown in figure 1. Light from a point source is collimated by a lens, passes through the test section, and is then focused to a point in the focal plane by an objective lens. Light scattered anywhere in the test section at an angle θ intersects the focal plane at a distance y from the focal point. Thus,

$$\theta = y/f \tag{1}$$

for $y/f \ll 1$, where f is the lens focal length. At the focal plane, a plate with a pinhole area δA subtends a cone with apex at the lens and with its axis in direction θ. The radiant power received by the area δA determines the irradiance as $H = P/\delta A$, power/area. The intensity in direction θ is $I = Pf^2/\delta A$, power/steradian. Thus, the intensity and irradiance are related by only a constant as

$$H = I/f^2 \tag{2}$$

This conversion is useful when calculating the power available to a detector at a given intensity. The scanning pinhole in figure 1 thus transmits the irradiance distribution which is proportional to the intensity distribution at the test section by equation (2).

To scan over a range of the angle θ, one or more pinholes may be part of a rotating disc to produce a periodic electrical waveform. Or, an image-type detector may be used to obtain nonmechanical scanning.

An alternative scanning slit assembly that has an area δA proportional to angle θ is shown in figure 2. It consists of a fixed V-shaped aperture and a slit that is translated in a radial direction. This produces a weighting factor proportional to θ that multiplies the intensity distribution provided by the scanning pinhole alone. (Since the radial translation of the scanning slit is mechanically awkward, the slit is usually cut into a motor-driven rotating disc; a weighting factor proportional to θ can be maintained with less than one percent error by using the curved aperture shown in fig. 3.)

The intensity distribution of the scanning pinhole and the scanning-slit assembly will be compared.

Intensity Distributions

Useful approximations for the intensity distribution of forward-scattered light in the center lobe (the lobe with maximum intensity at $\theta = 0$) are plotted in figure 4. The ordinate is the intensity at a scattering angle θ divided by the intensity at $\theta = 0$, the direction of the incident light. The abscissa is a beam-spread parameter $(\alpha\theta)^2$ where the particle size parameter is

$$\alpha = \pi D/\lambda. \tag{3}$$

with particle diameter D and wavelength λ.

The curve for a monodispersion is given by the Fraunhofer diffraction formula (ref. 1) as

$$\frac{I(\theta)}{I(0)} = \left[\frac{2J_1(\alpha \sin \theta)}{\alpha \sin \theta}\right]^2 \tag{4}$$

where J_1 is the first-order Bessel function. For $\theta < 20°$, $\sin \theta$ may be replaced by θ in radians.

The two curves for a polydispersion of particles are based on the Sauter mean diameter D_{32}. This diameter is the ratio of the third moment to the second moment of the particle-number distribution. The curves were derived in references 7 and 8 using equation (4) with a variety of particle-number distributions in which no particles exist with a diameter larger than a given multiple of that diameter at which the derivative dn/dD is a maximum.

The Gaussian curve is a good approximation to the other curves, and it will be used for error analysis, because of mathematical convenience.

Figure 5 shows the Gaussian relative intensity curve of figure 4 plotted with abscissa $\alpha\theta$ instead of $(\alpha\theta)^2$, and also another curve in which the ordinates have first been multiplied by a weighting factor proportional to θ (as would be produced by the scanning-slit assembly) and then normalized to a maximum value of unity for the relative intensity. One significant difference is apparent. With the scanning slit the maximum of the curve is moved away from $\alpha\theta = 0$ to $\alpha\theta \approx 1.25$. If particle diameter is to be inferred from the angle at which the weighted intensity is a fixed fraction of its maximum value, only one angle must be measured accurately. For example, if the intensity ratio is chosen to be 0.4, then $\alpha\theta$ must be 2.6. The angle at the broad maximum is not explicitly measured; instead, only the amplitude of the weighted intensity maximum is needed. In this sense, only the one angle at a fraction of the maximum is measured.

Measurement of the maximum and the angle θ at a fraction of maximum can be made in real time with an electrical waveform peak detector as used in reference 2; or, with a small time delay, by computer using one of several commercially available instruments designed for electrical waveform acquisition, storage and processing. The latter method is usually preferred.

The extraneous light produced by diffraction at the test section aperture is substantially ignored by the type of measurement described above, as shown by the following analysis.

Diffraction by Test-Section Aperture

Our tests of a forward-scatter optical system have shown that a fundamental limitation to measurement accuracy is extraneous light produced by diffraction of the light at the test section aperture even when the instrument optics produce negligible extraneous light by reflection or scatter.

The intensity distribution described by the Fraunhofer diffraction equation (4) applies both to the spray particles and to the test-section aperture. The existence of diffraction by the aperture is often ignored or overlooked. The methods used in references 11 and 12 eliminate the effect of diffraction by the aperture as well as the effect of other sources of interfering light. These methods may be considered when extraneous light is a major problem not controlled by the present method.

Because the test-section aperture diameter is much larger than a particle diameter, the aperture produces more scattered flux than does a small number of particles. This flux has a strong effect on the resultant intensity distribution as measured.

The Fraunhofer equation gives the intensity as:

$$I(\theta) = \frac{H\lambda^2\alpha^4}{16\pi^2}\left[\frac{2J_1(\alpha\theta)}{\alpha\theta}\right]^2 \tag{5}$$

where H is the irradiance of a plane wave of radiation at the aperture.

The Bessel function J_1 has peak values, the first one beginning at $\alpha\theta = 1.84$, that are closely approximated by an asymptotic formula (ref. 13):

$$J1(\alpha\theta) = (2/\pi\alpha\theta)^{1/2}\cos(\alpha\theta - 3\pi/4) \tag{6}$$

Equation (6), with the cosine factor replaced by unity (its maximum possible value), is substituted in equation (5) to yield an approximate envelope of the intensity peaks for $\alpha\theta \geq 1.84$. Along this envelope, for $\alpha\theta \geq 1.84$,

$$I(\theta) = \left(\frac{H\lambda^2}{16\pi^2}\right)\left(\frac{8\alpha}{\pi\theta^3}\right) \tag{7}$$

Figure 6 shows in solid lines the relative intensity $I(\theta,D)/I(0,d_0)$ as a function of angle θ, for a uniformly illuminated circular aperture or spherical particle of diameter D(when d_0 = 10 000 μm = 1 cm) as measured by a scanning pinhole. For $\alpha\theta > 1.84$, the intensity has been computed by equation (7). For $\alpha\theta < 1.84$, the intensity has been computed by equation (5). For $\alpha\theta < 1.84$, the two formulas yield the same numerical value within 2 percent.

To determine particle size solely from two intensity measurements, one makes measurements in that part of the center scattering lobe which corresponds to the knee of the curves. For a single particle and a circular aperture, figure 6 shows that at the knee of the curves for smaller diameter particles the intensity due to the uniform beam is greater than that due to the particle by a factor equal to the ratio of the aperture to particle diameter. This is undesirable because the uniform beam intensity overpowers the particle intensity. However, the situation can be improved by reducing the intensity diffracted at the aperture by use of aperture apodization, treated in reference 14.

Alternatively, instead of using a circular aperture with uniform irradiance, the irradiance may be made to decrease with distance from the optical axis. A laser beam, with the usual Gaussian irradiance distribution, has this property. The laser beam is optically expanded to a desired diameter at the test section. The Gaussian beam may be nominally sized by the "diameter" at which its irradiance is some fraction of the axial irradiance. In figure 6 the dotted lines apply to a Gaussian beam for which the irradiance amplitude ratio H/Ho is 0.5 at a diameter of 1.0 cm. For this beam, an aperture of diameter d = 1, 2, or 2.58 cm would produce H/Ho equal to 0.5, 0.0625, or 0.01 respectively. The improvement shown by the dotted line curves for these three aperture diameters is substantial and rapid at small scatter angles, after which an asymptotic slope $1/\theta^3$ is followed. The computation was done with the method of reference 15; that is, by a summation of Bessel functions of integer order instead of by analytic integration.

The gains obtained by apodization are also possible by spatial filtering (references 3, 16, and 17) but with a more complicated optical system.

For an unweighted measure of the spray, with uniform irradiance, and to minimize the weighting by a Gaussian beam, the beam in the test section should be rectangular. Thus, a circular aperture may be reduced by a wide slit with the long dimension oriented perpendicular to the direction of the spray velocity. The slit edge diffraction will be small in the direction nearly parallel to the slit edge. This modification is recommended.

Figure 6 shows that the intensity ratio would be very low if one sought to measure a single small-diameter particle. However, in the application considered here, there is a constant volume flow rate of liquid, and the number of small-diameter particles becomes very large.

The transmission factor is related to the number of particles, and there is a gain in intensity of the scattered light when N particles are present. If N particles of diameter D_p are distributed in a test section of diameter D_b, the transmission factor (ref. 10) is:

$$\tau(N) = \exp\left(\frac{-KN\pi D_p^2/4}{\pi D_b^2/4}\right) \tag{8}$$

where K is the scattering coefficient of a particle, equal to 2 for a particle diameter larger than the wavelength. When $K = 2$, some of the flux intercepted by the cross-sectional area is scattered by reflection and refraction through the particle, and an equal amount of flux is Fraunhofer diffracted on passing outside the particle. Thus, the diffracted radiation from N particles is equal to one-half the flux removed from the beam, and is a fraction $[1 - \tau(N)]/2$ of the incident light. The gain over the light intensity from one particle is thus:

$$\frac{1 - \tau(N)}{1 - \tau(1)} = \frac{1}{2}\,[1 - \tau(N)]\left(\frac{D_b}{D_p}\right)^2 \tag{9}$$

where, since $\tau(1)$ is near unity, the first two terms of the series approximation of τ are adequate to replace the denominator of equation (9), and K has been set equal to 2.

The intensity produced by the test section aperture is reduced by the transmission factor $\tau(N)$. Thus, the overall effective gain in intensity is the gain in equation (9) times $1/\tau(N)$:

$$G = \frac{[1 - \tau(N)]}{2\tau(N)}\left(\frac{D_b}{D_p}\right)^2 \tag{10}$$

If a single droplet were replaced by N droplets having the same total volume, the number N of droplets would vary inversely with the cube of droplet diameter. For example, if one droplet were 10^3 μm in diameter there would be 10^3 or 10^6 droplets of diameter 100 or 10 μm, respectively. Table I shows how the values of τ and G would change with diameter. The intensity ratio for this example is shown by the dashed lines in figure 6. The favorable results are:

(1) A large reduction in the range of variation of relative intensity with droplet diameter.

(2) At the knee of the curve, the effect of the aperture, for uniform illumination, is negligible for droplet diameters less than 10^2 μm. For Gaussian illumination with H/Ho = 0.0625, the effect of the aperture is small for droplet diameters less the 10^3 μm (0.1 the beam diameter). Thus, a large range of droplet diameters can be measured.

An unfavorable result is that the transmission factor in table I is less than 0.2 for 10-μm diameter particles. Multiple scatter at small values of τ can cause a smaller measured mean diameter as shown by reference 18.

To apply to the scanning-slit method, the ordinate of the solid-line curves of figure 6 is multiplied by a weighting factor of 1000 Θ to produce the solid-line curves of figure 7. A result evident from figure 7 is that the measured intensity due to particles changes very little with particle diameter. This helps measurement over a large range of diameters.

Effects of the Form of the Distribution Function and of the Dispersion

The intensity distribution with a scanning pinhole (fig. 4), was shown by references 7 and 8 to be relatively insensitive to the form of the particle number distribution function. It is necessary to find if this is also true for the intensity distribution with the scanning slit (fig. 5). In the following discussion particle volume distribution will be used instead of number distribution because it is a more widely accepted measure of spray produced by nozzles. Four forms of distribution functions as described by reference 19 will be used: Rosin-Rammler (RR), Nukiyama-Tanasawa (NT), log normal (LN), and Upper Limit Distribution Function (ULDF). The ULDF will be used with two values of the upper limit. Two more functions not so well known will also be used: Weibull, reference 20 and Rinkes, reference 21.

A cross-section of the spray near a nozzle has a mean particle diameter on axis, that may progress to a substantially different mean diameter off axis. Such a spray has a volume distribution different from the six functions to be used. This distribution will not be considered because it is more correctly determined by measurements with a narrow laser beam at a number of distances from the spray axis. These measurements may then be inverted to give the mean diameter as a function of distance from the spray axis. An appropriate inversion method is described by reference 22.

The spread of any one distribution curve will be characterized by the dispersion Δ_V, where

$$\Delta_V = 2(D_{V0.9} - D_{V0.1})/(D_{V0.9} + D_{V0.1}) \qquad (11)$$

and where $D_{V0.1}(D_{V0.9})$ = particle diameter such that one tenth (nine tenths) of the total volume of all drops is composed of drops smaller in diameter than $D_{V0.1}(D_{V019})$.

If $\bar{D}$ represents the diameter at which the distribution is a maximum and if the distribution functions are normalized so that this maximum is unity, the

six distribution functions appear as plotted in figure 8, for an arbitrary diameter $\bar{D}$ = 50 μm, and a dispersion Δ_V = 1.35. This dispersion represents the widest usually produced by a spray. These distributions are considered to bound the actual distribution produced by a spray nozzle. The curves are represented by the following formulas in which δ = distribution parameter, and $x=D/\bar{D}$; $z=(dV/dD)/(dV/dD)_{\bar{D}}$

(1) Rosin-Rammler, RR,

$$z = \varepsilon^{A-Bx^{\delta-1}} \tag{12.1}$$

where

$A = (\delta-1)/\delta$

$B = Ax^{\delta}$

(2) Nukiyama-Tanasawa, NT,

$$z = \varepsilon^{A-Bx^5} \tag{12.2}$$

where

$A = 5/\delta$

$B = Ax^{\delta}$

The RR and NT functions are identical when $\delta - 1 = 5$.

(3) Log Normal, LN,

$$z = x^{-1}\varepsilon^{(A^2-B^2)}$$

where

$$A = 0.5\delta \qquad B = \delta \cdot \ln x - A \tag{12.3}$$

(4) Upper Limit Distribution Function, ULDF, where D_U is the largest particle diameter,

$$z = \varepsilon^{(A^2-C^2)/(Bx)} \tag{12.4}$$

where

$x_u = Du/\bar{D}$

$A = \frac{1}{2} - \frac{1}{x_u}$

$B = (x_u - x)/(x_{u-1})$

$C = \delta \cdot \ln(Bx\varepsilon^{-A})$

(5) Weibull,

$$z = \varepsilon^{A-B_x\delta+2} \tag{12.5}$$

where

$A = (\delta + 2)/\delta$

$B = Ax^{\delta}$

The Weibull is identical to the RR when $\delta + 2$ is replaced by $\delta - 1$. The Weibull is identical to the NT when $\delta + 2 = 5$.

(6) Rinkes,

$$z = (A/x^2)\varepsilon^{-B(1-x)/x} \tag{12.6}$$

where

$A = (\delta - x)/(\delta - 1)$

$B = (5\delta - 4)/(\delta - 1)$

$\delta = D_U/\bar{D} = x_U$

The quantity D_U is the upper limit of particle diameter. The parameter δ in these distribution functions governs the spread in particle diameters. The relation between the dispersion Δ_V and the δ's in the various functions given by equations 12.1 to 12.6 is shown in figure 9.

As shown by reference 19 the RR function has unreasonable values of mean diameter. The cause for this is shown by the relative number distribution plotted in figure 10. The curves have been normalized so that they have a maximum of unity. The RR and Weibull functions go to infinity at zero diameter for this large dispersion; consequently they have been truncated, so that they remain at a value of zero for all diameters D less than $D_\ell = 0.1$ μm ($D_\ell/\bar{D} = 0.005$).

The effect of the various distributions on various definitions of mean diameter $D_{p,q}$ is shown in figure 11 for all combinations of p and q for which $p + q \leq 5$. Three truncation points have been assumed for the RR function; only the truncation at $D_\ell = 2$ μm ($D_\ell/\bar{D} = 0.025$) appears to yield realistic values of mean diameter, comparable to those yielded by the other distribution functions. The RR function will therefore be used with truncation at $D_\ell/\bar{D} = 0.025$. The Weibull function will be accepted, with truncation as shown in figure 10, at $D_\ell/\bar{D} = 0.002$.

Figure 12(a) shows the scattered-light-intensity distributions for the seven distributions assuming a constant value of $D_{V0.5}$, and three values of the dispersion Δ_V. For any one value of dispersion, all intensity distributions are sufficiently alike so that only the envelope of each band of curves is shown. For $\Delta_V = 0.1$, the band is so narrow that only a single curve need be drawn. Distributions are shown both for a scanning pinhole (with ordinate I/I_{max}) and for a scanning slit (with ordinate $I_w/I_{w,max}$). Figure 12(b) shows a similar set of distributions assuming a constant value of D_{32}, figure 12(c) is for a constant value of $D_{V0.75}$, and figure 12(d) is for a constant value of D_{31}.

The abscissa in figure 12 is the beam spread parameter $\alpha\theta$. The maximum spread in the value of the abscissa at any ordinate, after all distribution functions and all dispersions are considered, may be represented by the maximum fractional deviation $\Delta(\alpha\theta)/(\alpha\theta)$.

In figure 12, the value of the ordinate at which there is smallest dependence on the dispersion and on the distribution function is determined as follows: A median curve is drawn for each pair of envelopes (for $\Delta_V = 0.1$, the curve drawn is already the median); the point sought is taken as the center of area of the triangle formed by the three points of intersection of the three median curves. (For greater accuracy in determining the centroid, the curves were redrawn to greatly enlarged scale in the vicinity of the intersections; however, these enlarged curves are not shown here.) In figure 12(c), for the scanning slit, the median curves are closest together on the left of the maximum. The following conclusions result.

(1) The coordinates of the points of the smallest dependence are as listed in table II, which also lists the maximum spread $\Delta(\alpha\theta)/(\alpha\theta) = \Delta\theta/\theta$ in the abscissas of those points.

(2) If intensity measurements are made at these points, the value of $D_{v0.5}$ and $D_{v0.75}$ will be less dependent on the choice of volume distribution function than will the value of D_{32}. This conclusion holds regardless of whether the scanning slit or the scanning pinhole is used.

(3) The use of the scanning slit requires measurements of $\Delta\theta$ at a much larger fraction of the maximum intensity than does the use of the scanning pinhole. This improves accuracy of measurement.

(4) Away from the selected values of $\Delta(\alpha\theta)$ listed in (1), there is a strong dependence on particle volume dispersion. This result does not agree with the conclusions of references 7 and 8, because the dispersion was not varied over a wide range, in those reports.

(5) The envelopes of figure 12 are bounded principally by the RR on the lower part and by the Rinkes on the upper part, following the progression of D_{pq} in figure 11. When the distribution function is not known, one may choose a typical function near to the center of the group like the NT or the ULDF with $D_U/\bar{D} = 10$.

The abscissas of all measurement points listed under 1(a) to 1(g) lie between 0.9 and 3.3. In order to clarify the dependence on dispersion, the curves of figures 12(a) to (d) have been redrawn in figure 12(e) so that they pass through a common intersection point at an abscissa of $\alpha\theta = 2.5$ with an intensity ratio of 0.4 for the scanning slit and of 0.04 for the scanning pinhole. The common intersection point was produced by letting the diameter $\bar{D}$ of each function deviate from 50 μm. The envelopes are thereby condensed to show explicitly the effect of dispersion and of the function (principally skewness of the function). At the intersection, the slope of the envelopes shows a significant change with dispersion. The width $\Delta(\alpha\theta)$ of an envelope even at the largest dispersion is narrow relative to the change of $\alpha\theta$ with dispersion. Because the envelope contains the curves of all functions, this method is insensitive to the distribution function.

Dispersion of Particle Volume Distributions

For any one curve, we shall define, for the scanning slit, a slope parameter (s_f) as

$$s_f = \frac{\dfrac{\left(I/I_{max}\right)_{32}}{\left(I/I_{max}\right)_{v0.5}} - 1}{\dfrac{(\alpha\theta)_{32}}{(\alpha\theta)_{v0.5}} - 1} = \frac{-0.42}{\dfrac{(\alpha\theta)_{32}}{(\alpha\theta)_{v0.5}} - 1} \tag{13}$$

where

$(I_w/I_{w,max})_{v0.5} = 0.73$ = optimum intensity ratio for measurement of $D_{v0.5}$

$(I_w/I_{w,max})_{32} = 0.42$ = optimum intensity ratio for measurement of D_{32}

$\theta_{v0.5}$ = angle at which $(I_w/I_{w,max})_{v0.5} = 0.73$

θ_{32} = angle at which $(I_w/I_{w,max})_{32} = 0.42$

Using the defintion of Δ_v given by equation (11), the plot in figure 13 shows the mean value of $s(\Delta_v)$ and, by the bars at the various points, the spread in the values of s for the seven distribution function shown in figure 10. Figure 13 shows an excellent correlation between s_f and Δ_v that is substantially independent of the volume distribution function. Thus, figure 13 may be used to determine the volume dispersion Δ_v. Figure 9 may then be used to determine the parameter δ for any of the functions in equations 12.1 to 12.6 if these are of interest. The average deviation (a.d.) of individual points from the curve drawn in figure 13 is 0.4 times what the a.d. would be if $2D_{v0.5}$ were used in the denominator of equation (11) instead of $(D_{v0.9} + D_{v0.1})$.

Procedure for Treatment of Experimental Data

The preceding analysis leads to the following analytical treatment of experimental data obtained by the scanning-slit apparatus. (Note that this apparatus yields I_w as a directly measured quantity.)

(1) By varying angle θ, the maximum weighted intensity $I_{w,max}$ is found and recorded.

(2) By varying angle θ, the angles $\theta_{v0.5}$ and θ_{32} are found at which I_w has a value given by $I_{w,max}$ × (ordinate listed in table II). These angles are recorded.

(3) The slope factor s is computed by equation (13) and the dispersion Δ_v then determined from figure 13.

(4) The diameters $D_{v0.5}$ and D_{32} are computed from the measured angles $\theta_{v0.5}$ and θ_{32} and the abscissa values listed in table II.

(5) Operations like steps 2 and 4 may also be used to compute $D_{V0.75}$ and D_{31}, if they are of interest.

An alternative procedure that leads directly to the relation between particle diameter and angle, is possible if there are available several slides, each of which has a monodispersion of representative particles in the diameter range of interest. With apparatus like that to be described later under Experimental Simulations, such calibration can be more accurate than step 4, above.

A correction of the measured slope for possible instrument error may improve accuracy. When diameter calibration is made with microspheres having dispersion near 0.16, the measured slope may be compared with s_f in figure 13 and equation (13) to determine a correction.

Two additional refinements are possible. One is a correction for the case where particle diameters are so small that Mie's treatment of diffraction phenomena is significantly superior to Fraunhofer's method. The other is a correction for multiple dispersion when particle density is high. These two corrections will now be considered.

Corrected Computation Based on Mie Diffraction

Up to this point, the dispersion and four mean diameters have been determined analytically assuming Fraunhofer diffraction. However, for small diameter, Mie's treatment of diffraction is necessary to obtain a true intensity distribution. Such a computation has been made for the scanning-slit method, and the results expressed in the form of corrections to be applied (iteratively, if desired)

(1) To the value of the ordinate to be entered into figure 13, in order to find a closer value of Δ_V, and
(2) To the value of the originally computed mean diameter, in order to find a closer value.

The procedure of the computation followed that which was used to obtain figures 12 and 13. For the seven distributions previously assumed, and for five values of dispersion, the parameters $(\alpha\theta)$ at the four ordinates listed in table II, and the corresponding slope factor s computed from equation (13), were determined. Calling these quantities $(\alpha\theta)_M$ and s_M, respectively, and calling the respective original values $(\alpha\theta)_F$ and s_F, figures 14 and 15 result for Mie scatter with water.

The corrected procedure then becomes:

(1) Use the original procedure (steps 1 through 4) to obtain first estimates of dispersion Δ_V and mean diameters $D_{V0.5}$ and D_{32}.

(2) Use the measured slope s_M and the equation in figure 14 to find s_F/s_M. Then compute an equivalent s as

$$s = (s_F/s_M) \times s_M$$

and enter this value of s into figure 13 to find a corrected Δ_V.

(3) Use figure 15 to find a corrected mean diameter from a corrected value of θ given by

$$\theta = (\theta_M/\theta_F \text{ from fig. 15}) \times (\text{measured } \theta)$$

This last step is not necessary if an experimental calibration is available with microspheres in the range 3 to 12 μm.

The graphs of figures 14 and 15 represent computed points joined by straight lines. Each point is the median among the seven assumed distributions. Vertical bars at the points represent the spread among the seven distributions. At the right-hand end of figure 14 are shown the original values of s_F and their associated spreads when Fraunhofer diffraction had been assumed. Similarly, the spreads among the seven distributions are shown in figure 15, along with the value of $\Delta\theta_F/\theta_F$ from table II.

The following deductions are noteworthy:

(1) Corrections become significant only when mean diameter is less than 12 μm.

(2) For $\Delta_V > 0.5$ and $D_{V0.5} < 3$ μm, the differences among the curves are comparable to or smaller than the spread for any one curve. Consequently, the lower limit of mean diameter is 3 μm, unless Δ_V is known by other means.

(3) The spreads among the distributions are acceptably small. The spreads in s_M are comparable to those in s_F; the spreads in angle θ assuming Mie diffraction are smaller than the spreads assuming Fraunhofer diffraction.

Multiple Scatter Correction

A model of multiple scatter was derived by reference 18, based on Fraunhofer diffraction. Correction factors were presented for a Rosin-Rammler distribution that determine diameter D and the dispersion parameter δ from the measured D_m, δ_m, and transmission factor τ. The correction factors are $C_D = D/D_m$ and $C_\delta = \delta/\delta_m$. An exact correction like that obtained for Mie scatter would include seven distributions and four average diameters. In order to apply the method of reference 18 to this paper, two variables in the correction equations of reference 18 were replaced by the variables used in this paper.

(1) The dispersion parameter N or δ was replaced by Δ_V using the RR function in figure 9.

(2) The obscuration $OB = 1 - \tau$ was replaced by τ.

The two resulting equations and graphs of the equations of reference 18 are shown in figure 16.

The equations may be applied after the correction for Mie diffraction from the preceding section has yielded the corrected values of mean diameter and dispersion. The same correction is applied to all four diameters.

One limitation of the multiple scatter correction is the assumption of a transmission factor that is constant for every ray in the laser beam. This condition is not met with an axisymmetric spray where the transmission faactor is unity at the edge of the spray envelope, and much smaller near the centerline. To minize this source of error the laser beam cross-section should be adjusted to lie within the spray envelope. An alternative technique is first to use a fixed large diameter laser beam tc determine the mean diameter then to make the beam narrow in order to determine the transmission factor that can be used to determine the multiple scatter correction.

ERROR ANAL'SIS

Gaussian Approximation cf Scattered Light

In figure 17 the light scattered by particles and transmitted by the scanning slit has a maximum weighted intensity $I_{w,max}$ at angle θ_1, and a weighted intensity $I_{w,2}$ at a fixed fraction of $I_{w,max}$ at angle θ_2. Weighted intensity I_w will be taken as irtensity I multiplied by θ.

Using the Gaussian approximation of scattering (fig. 4) for the intensity I, the multiplied intensity is

$$I_w = \theta I = \theta \exp[-(aD\theta)^2] \tag{14}$$

where $a = 0.57\ \pi/\lambda$, $aD/0.57 = \alpha$, and θ is in radians.

The intensity ratio $I_{w,2}/I_{w,1}$ at angles θ_2 and θ_1 is

$$I_{w,2}/I_{w,max} = (\theta_2/\theta_1) \exp\left[-(aD)^2\left(\theta_2^2 - \theta_1^2\right)\right] \tag{15}$$

Angle θ_1 can be eliminated from equation (15) because θ_1 is the angle at which I_w is a maximum. At this maximum

$$\theta_1^2 = 0.5(aD)^2 \quad \text{and} \quad I_{w,max} = (aD\sqrt{2\varepsilon})^{-1} \tag{16}$$

Thus, equation (15) becomes

$$I_{w,2}/I_{w,max} = \sqrt{2\varepsilon}\ aD\theta_2 \exp[-(aD\theta_2)^2 \tag{17}$$

Figure 4 may be used to apply to the scann ng-slit method if $(\alpha\theta_2)^2$ is used as the abscissa and $(I_{w,2}/I_{w,max})/(aD\theta_2\sqrt{2\varepsilon})$ s used as the ordinate.

Equation (17) shows that, at any intensity ratio, the diameter D varies inversely with θ_2; however, an explicit solution for D is not possible.

Differentiating equation (17) gives the error in D caused by error in intensity measurement:

$$\frac{dD}{D} = \frac{(dI_{w,2}/I_{w,2}) - (dI_{w,max}/I_{w,max})}{1 - 2(aD\theta_2)^2} \tag{18}$$

when θ_2 is measured with neglible error. Because the various sources of extraneous light are independent of I, we assume that the random error in intensity measurement is constant and not dependent on I, and that the variances $(dI_{w,max})^2$ and $(dI_{w,2})^2$ may each be set equal to $(dI_w)^2$.

Then equation (18) can be written as

$$\left|\frac{dD/D}{dI_w/I_w}\right| = \frac{\left[1 + (I_{w,max}/I_{w,2})^2\right]^{1/2}}{\left|1 - 2(aD\theta_2)^2\right|} \quad . \tag{19}$$

Equations (17) and (19) may be treated as parametric equations, with the common parameter $aD\theta_2$, so that the error ratio on the left side of equation (19) may be represented as dependent solely on the ratio $I_{w,2}/I_{w,max}$. For $\theta_2 > \theta_1$, the error ratio plotted in figure 18 shows a broad minimum between intensity ratios of 0.15 and 0.80. For $\theta_2 < \theta_1$ the error ratio plotted in figure 18 shows a broad minimum between intensity ratios of 0.15 and 0.80. For $\theta_2 < \theta_1$, there is a narrower minimum between intensity ratios of 0.55 and 0.85. The value of 0.85 is chosen to measure $D_{V0.75}$ because it gives the largest measurement angle and thereby minimizes the effects of extraneous light caused by diffraction by the test section aperture.

The minimum error is comparable to the minimum error of the two methods that were compared in reference 3, but with the important advantage that particle diameter does not appear in figure 18.

EXPERIMENTAL SIMULATIONS

Confirmation of theoretical calculations appears possible by optical-laboratory experiments in which the spray and the background are simulated by glass plates carrying a dispersion of microspheres. In the experiments to be described, the measurements were made with a commercially available digital instrument designed for electrical waveform acquisition, storage, computation, and display, with output to a printer and a plotter. At the time of this test, a scanning pinhole was used instead of a scanning slit.

Microsphere Calibration Plates and Mounting

Polystyrene latex microspheres suspended in water are commercially available, reference 23. A calibration plate is made by depositing the particles on a microscope cover slide preferably coated for minimum reflectance at the laser wavelength.. A typical coating is shown in figure 19 for 100 μm particles on both sides of the slide. The transmission factor of the particles on the slide is 0.85, or 0.92 for each side. To obtain a lower transmission factor, two slides are mounted 1 cm apart in a protective housing. To divert light that is multiply reflected by the slide surfaces, away from the detector, the two slides are inclined at an angle of 0.01 rad to each other, and the assembly is inclined at 0.01 rad or more to the plane-parallel test section windows. The two test section windows are also inclined at 0.01 rad to each other. Each slide is selected to have sides parallel to each other to 0.0001 radian as determined by inspection of interference fringes with a sodium vapor lamp.

A spray chamber to deposit particles on a microscope slide is shown in figure 20. An artists airbrush spray-gun atomizes a suspension of microspheres in a liquid that has the same density as the particles. The liquid mixture is approximately 10 cc propanol, 6 cc Freon cleaning fluid, and 1 cc water containing the particles. Enough particles are included to produce a clouded mixture when viewed against a white background. The air brush fluid flow rate is adjusted by observing the spray-scattered light from the two microscope illuminators. The upper illuminator shows the existence of spray. The lower illuminator shows the degree of evaporation of the spray. The spray falling on the microscope slide must be sufficently evaporated to avoid formation of a liquid film on the slide, which will cause the particles to migrate and form clumps. Insufficient flow of spray will tend to produce dry particles or dust that does not accumulate on the slide. The concentration of particles on the slide is limited to that shown in figure 19. An attempt for greater particle concentration causes particles to accumulate on top of those already deposited.

Analytical Correction for Extraneous Light

In figure 21(a), a collimated laser beam with intensity I_o is incident on a test section containing no spray. Some of the light transmitted through the test section is not scattered. It has an intensity $I_o\tau_o$ where τ_o is the transmission factor of the test section, including test section windows.

A fraction of the light is forward-scattered with an intensity $I_o\tau_o k_o$ that is a fraction k_o of the intensity of the axially-transmitted beam. The scattered-light intensity is usually less than one percent of the axial intensity.

Separate detectors are used for the axial beam and for the scattered beam; these have calibration factors c_b and c_a, respectively, each representing intensity per unit detector voltage. Equations (20) and (21) give the two detector voltages: E_o for the axial beam and $e_o(\theta)$ for the beam scattered at angle θ.

$$c_a e_o(\theta) = I_o\tau_o k_o(\theta) \tag{20}$$

$$c_b E_o = I_o\tau_o \tag{21}$$

In figure 21(b) spray has been added to the test section. Both the scattered and unscattered-light intensities given in equations (20) and 21) are equally attenuated by the spray particles with a transmission factor τ_s; the complementary part $1 - \tau_s$ is scattered by the spray in all directions. In the forward direction, the presence of spray adds to the scattered light an intensity $I_o\tau_o k_s(\theta)$. The detector voltages are now $e_m(\theta)$ and $E_m(0)$ given by equations (22) and (23) as

$$c_a e_m(\theta) = I_o\tau_o\tau_s k_o + I_o\tau_o k_s(\theta) \tag{22}$$

$$c_b E_m = I_o\tau_o\tau_s \tag{23}$$

The desired quantity is $I_o\tau_o k_s(\theta)$ for the spray alone. This is obtained by combining equations (20) through (23) to obtain

$$I_o\tau_o k_s(\theta) = c_a e_m(\theta) - \tau_s c_a e_o(\theta) \tag{24}$$

where the spray transmission factor is

$$\tau_s = E_m/E_o \tag{25}$$

The desired intensity $I_o\tau_o k_s(\theta)$ alone would produce in the absence of background, a voltage $e_s(\theta)$ is given by:

$$I_o\tau_o k_s(\theta) = c_a e_s(\theta) \tag{26}$$

Substitution of equation (26) in (24) gives the voltage distribution for the spray, corrected for background light,

$$e_s(\theta) = e_m(\theta) - \tau_s e_o(\theta) \tag{27}$$

This is the general equation for correction of background light by subtraction of functions of θ.

The validity of equation (27) was determined by a test with the microsphere calibration plates. If two plates are put in the test section (fig. 21(c)), one plate can be treated as an added cause of background light, and the other plate treated as spray. The intensity due to background can thus be made greater than the intensity due to spray in order to to exaggerate the needed correction. Both plates were first measured separately. For the background plate (plate 1, subscript 1), the detector voltages analogous to equations (22) and (23) with subscript 1 in place of subscripts s and m, are given by:

$$c_a e_1(\theta) = I_o\tau_o\tau_1 k_o(\theta) + I_o\tau_o k_1(\theta) \tag{28}$$

$$c_b E_1 = I_o\tau_o\tau_1 \tag{29}$$

For the second plate (plate 2, subscript 2) alone, equations (28) and (29) change to

$$c_a e_2(\theta) = I_o\tau_o\tau_2 k_o(\theta) + I_o\tau_o k_2(\theta) \tag{28b}$$

$$c_b E_2 = I_o\tau_o\tau_2 \tag{29b}$$

With both plates in the test section (fig. 21(c)) the intensities shown in the figure produce voltages given by:

$$c_a e_3(\theta) = I_o\tau_o\tau_1\tau_2 k_o(\theta) + I_o\tau_o\tau_2\tau_2 k_1(\theta) + I_o\tau_o\tau_1 k_2(\theta) \tag{30}$$

and

$$c_b E_3 = I_o\tau_o\tau_1\tau_2 \tag{31}$$

The desired intensity is represented by $I_o\tau_o k_2(\theta)$. Analogous to equation (26), a voltage that would correspond to this intensity alone, if there were zero background, is represented by $e_s(\theta)$ where

$$c_a e_s(\theta) = I_o\tau_o k_2(\theta) \tag{32}$$

Combination of equations (28), (30), and (32) yields

$$e_s(\theta) = [e_3(\theta) - \tau_2 e_1(\theta)]/\tau_1 \tag{33}$$

where

$$\tau_1 = E_1/E_o \qquad \tau_2 = E_2/E_o \tag{34}$$

A check on the experiment is that the product $\tau_1 . \tau_2$ should be equal to E_3/E_o.

Experimental Results

Measurements were made with calibration plates bearing 25- and 50-μm microspheres to simulate the background and the spray. The measured transmission factors of these plates were 0.650 and 0.661 respectively. Figure 22(a) shows the voltage distributions $e_o(\theta)$ with no plates, $e_1(\theta)$ with the 25-μm plate alone, $e_2(\theta)$ with the 50-μm plate alone and, $e_3(\theta)$ with both plates. The voltage ratio $E_3/E_o = 0.423$ with both plates is in good agreement with the product $\tau_1 . \tau_2 = 0.650 \times 0.661 = 0.429$.

Figure 22(b) shows the true distribution $e_s(\theta)$ for the 25-μm plate as determined by equation (33), when the 50 μm plate was used to simulate the background. A comparison curve for the 25-μm plate alone, using equation (27) shows a smoother distribution and presumably is more accurate. There is good agreement between the curves; the background is thus only one ninth of the total signal.

A second test of the equations is a comparison of the measurements of $e_2(\theta)$ using plate 2 alone with the calculation of $e_2(\theta)$ from measurements made where both plates are used. For the latter condition, equations (20), (28), and (30) give

$$\tau_1 e_2(\theta) = \tau_1 \tau_2 e_o(\theta) - \tau_2 e_1(\theta) + e_3(\theta) \tag{35}$$

The two curves for $e_2(\theta)$, shown in figure 22(c), show good agreement.

The correction for extraneous light is in error in the presence of turbulence or other causes of refraction induced by the gas flow in the test section. The introduction of spray may change the the magnitude of these refraction effects, as shown by reference 5. For example, when our tests showed small-angle refraction by turbulence, the addition of spray reduced the refraction, so that the correction for extraneous light at small refraction angles was excessive.

CONCLUSION

A scanning optical system and a technique of data analysis have been described that permit determination of average particle diameters in a spray of droplets over a wide range of diameter distributions and of diameter dispersions when there is a large aggregate of droplets. Mie computation shows a

diameter less than 3 μm cannot be accurately measured. Measurement of the angle at which the scattered-light intensity is 73 percent of the maximum intensity suffices to yield the volume median diameter. Measurement of the angle at which the scattered-light intensity is 42 percent of the maximum intensity suffices to yield the Sauter mean diameter. However, measurement of both of these angles and of the corresponding intensities at these angles also yields the dispersion of the volume size distribution. Measurement of the angle at which the scattered-light intensity is 85 percent of the maximum intensity yields the diameter at 0.75 of the cumulative volume. This diameter may be useful to measure the relative amount of large diameter particles. Measurement of the angle at which the scattered light intensity is 24 percent of the maximum intensity yields the volume/diameter mean D_{31}. This diameter may be useful when compared with D_{32} to better characterize the spray. The effect of extraneous light such as that introduced by the test section aperture may be reduced and corrected. The effect of multiple scatter may be corrected. Measurement of the spray transmission factor is needed to make both corrections. The effect of Mie scatter may be corrected. Use of a light source, like a laser, that produces a Gaussian distribution of off-axis irradiance improves accuracy.

A method of using latex microspheres deposited on glass plates to simulate the spray and the background has been described. It provides a means of calibrating the instrument and testing the measurement technique. Cross checks have indicated that the simulation is reliable.

APPENDIX - SYMBOLS

a	0.57
A	constant in distribution function
B	Constant in distribution function
c_a	calibration constant for off-axis-light detector
c_b	calibration constant for axial-light detector
C	constant in distribution function
D	diameter of particle on aperture
$\bar{D}$	diameter at which volume distribution function is a maximum
D_0	reference diameter
D_{20}	diameter at mean of surface-area
D_{30}	diameter at mean of volume
D_{31}	diameter at mean of (volume/diameter)
D_{32}	Sauter mean diameter (at mean of volume/area)
D_m	measured diameter
$D_{v0.5}$	volume median diameter, cumulative volume fraction 0.5
$D_{v0.75}$	diameter at cumulative volume fraction 0.75
$D_{v0.1}$	diameter at first decile of droplet volume distribution
$D_{v0.9}$	diameter at ninth decile of droplet volume distribution
D_b	test section diameter
D_f	diameter with Fraunhofer diffraction
$D_{m,s}$	diameter with microsphere calibration
D_p	particle diameter
D_u	upper limit of particle diameter
D_ℓ	lower limit of particle diameter
d	aperture diameter
E	voltage indicated by axial-light detector (a)

e	voltage indicated by scattered-light detector (b)
e_0, E_0	value of e,E when there is no spray
e_m, E_m	value of e,E where there is spray
e_s	value of e for spray alone
E_0 to E_3	value of E under conditions 0 to 3
e_0 to e_3	value of e under conditions 0 to 3
f	focal length of objective lens
G	gain in intensity
H	irradiance
H_0	irradiance in axial direction
I	radiant intensity
I_0	radiant intensity of axial beam
I_{max}	maximum radiant intensity
I_w	weighted intensity, $I\theta$
$I_{w,max}$	maximum weighted intensity
$I_{w,max}, I_{w2}$	weighted intensity at angle θ_1, θ_2
J_1	Bessel function of first kind
K	scattering coefficient for single particle
k	scattering coefficient
k_s	scattering coefficient for spray
k_0	scattering coefficient for empty test section
k_1, k_2	scattering coefficient for plate 1, plate 2
N	number of particles
n	number fraction of particles
P	radiant power
s_F	slope parameter by assuming Fraunhofer diffraction
s_M	slope parameter by assuming Mie diffraction

V	volume of particles
V_0	total volume of particles
x	$D/\bar{D}$
x_u	$D_u/\bar{D}$
y	ray displacement at focal distance f (fig. 1)
z	$dV/dD)/(dV/dD)_D$
$\alpha\Theta$	beam spread parameter
Δ_V	dispersion of volume distribution
$\Delta_{V,m}$	measured Δ_V
δ	parameter in distribution function
δ_m	measured δ
δA	area of scanning aperture (figs. 1 and 2)
ε	base of Napierian logarithms
θ	angular direction of forward-scattered ray
θ_1	angle at which maximum weighted intensity occurs
θ_2	angle at which weighted intensity is measured
θ_F	angle assuming Fraunhofer diffraction
θ_M	angle assuming Mie diffraction
$\theta_{m,s}$	angle with microsphere calibration
λ	wavelength of radiation

Subscripts

0	transmission factor of test section
s	transmission factor of spray
1	transmission factor for plate 1
2	transmission factor for plate 2
3	transmission factor for plates 1 and 2

REFERENCES

1. Hodkinson, J.R.: Particle Sizing by Means of the Forward Scattering Lobe. Appl. Opt., vol. 5, no. 5, May 1966, pp. 839-844.

2. Buchele, D.R.: Scanning Radiometer for Measurement of Forward-Scattered Light to Determine Mean Diameter of Spray Particles. NASA TM X-3454, 1976.

3. Buchele, D.R.: Particle Sizing by Measurement of Forward-Scattered Light at Two Angles. NASA TP-2156, 1983.

4. Cornillault, J.: Particle Size Analyzer. Appl. Opt., vol. 11, no. 2, Feb. 1972, pp. 265-268.

5. Swithenbank, J., et al.: A Laser Diagnostic Technique for the Measurement of Droplet and Particle Size Distribution. AIAA Paper 76-69, Jan. 1976.

6. Dodge, L.G.; and Cerwin, S.A.: Extending the Applicability of Diffraction-Based Drop Sizing Instruments. Liquid Particle Size Measurement Techniques, ASTM STP-848, J.M. Tishkoff, R.D. Ingebo, and J.B. Kennedy, eds., American Society for Testing and Materials, 1984, pp. 72-81.

7. Dobbins, R.A.; Crocco, L.; and Glassman, I.: Measurement of Mean Particle Sizes of Sprays from Diffractively Scattered Light. AIAA J., vol. 1, no. 8, Aug. 1963, pp. 1882-1886.

8. Roberts, J.H.; and Webb, M.J.: Measurement of Droplet Size for Wide Range Particle Distributions. AIAA J., vol. 2, no. 3, Mar. 1964, pp. 583-585.

9. Standard Practice for Determining Data Criteria and Processing for Liquid Drop Size Analysis. ASTM Standard E799-81(1985), American Society for Testing and Materials, 1987.

10. Gumprecht, R.O.; and Sliepcevich, C.M.: Scattering of Light by Large Spherical Particles. J. Phys. Chem., vol. 57, no. 1, Jan. 1953, pp. 90-95.

11. Spinrad, R.W.; Zaneveld, J.R.V.; and Pak, H.: Volume Scattering Function of Suspended Particulate Matter at Near-Forward Angles: A Comparison of Experimental and Theoretical Values. Appl. Opt., vol. 17, no. 7, Apr. 1, 1978, pp. 1125-1130.

12. Hard, S.; and Nilsson, O.: Laser Heterodyne Apparatus for Measuring Small Angle Scattering From Particles. Appl. Opt., vol. 18, no. 17, Sept. 1, 1979, pp. 3018-3026.

13. Hildebrand, F.B.: Advanced Calculus for Engineers. Prentice-Hall, 1949.

14. Jacquinot, P.; and Roizen-Dossier, B.: Apodisation. Progress in Optics, Vol. III, E. Wolf, ed., North-Holland, 1964, pp. 29-186.

15. Olaofe, G.O.: Diffraction by Gaussian Apertures. J. Opt. Soc. Am., vol. 60, no. 12, Dec. 1970, pp. 1654-1657.

16. Blodgett, J. A.; and Easton, R. L., Jr.: Two-Stage Spatial Filtering for Diffraction Pattern Analysis. Appl. Opt., vol. 20, no. 6, Mar. 15, 1981, pp. 1050-1055.

17. Hutzler, P.J.S.: Spatial Frequency Filtering and its Application to Microscopy. Appl. Opt., vol. 16, no. 8, Aug. 1977, pp. 2264-2272.

18. Felton, P.G.; Hamidi, A.A.; and Aigal, A.K.: Measurement of Drop Size Distribution in Dense Sprays by Laser Diffraction. ICLASS-85, Proceedings of the Third International Conference on Liquid Atomization and Spray Systems, Institute of Energy, London, 1985, pp. IVA/4/1 - IVA/4/11.

19. Mugele, R.A.; and Evans, H.D.: Droplet Size Distribution in Sprays. Ind. Eng. Chem., vol. 43, no. 6, June 1951, pp. 1317-1324.

20. Gouesbet, G.; and Ledoux, M.: Supermicronic and Submicromic Optical Sizing Including a Discussion of Densely Laden Flows. Opt. Eng., vol. 23, no. 5, Sept.-Oct. 1984, pp 631-640.

21. Kayser, A.: Optical Measurements of the Droplet Size Distribution in the Case of Fuel Atomization in Swirl Nozzles and Planar Airblast Diffusers. NASA TM-75334, 1978.

22. Hammond, D.C. Jr.: Deconvolution Technique for Line-of-Sight Optical Scattering Measurements in Axisymmetric Sprays. Appl. Opt., vol. 20, no. 3, Feb. 1, 1981, pp. 493-499.

23. Microspheres sold through Duke Scientific Corp., Palo Alto, Ca.

TABLE I. - NUMBER OF PARTICLES AT CONSTANT TOTAL VOLUME, AND A UNIFORMLY-ILLUMINATED APERTURE DIAMETER OF 10^4 μm WITH RESULTING TRANSMISSION FACTOR τ AND INTENSITY GAIN G

Diameter, μm	N	τ	G
10^3	1	0.980	1.01
10^2	10^3	.819	1.11×10^3
10^1	10^6	.135	3.20×10^6

TABLE II. - COORDINATES OF POINTS OF SMALLEST DEPENDENCE

Mean diameter	Scanning Slit			Scanning Pinhole		
	$I_w/I_{w,max}$	$\alpha\theta$	$\Delta(\alpha\theta)/(\alpha\theta)$	I/I_{max}	$\alpha\theta$	$\Delta(\alpha\theta)/(\alpha\theta)$
$D_{v0.5}$	0.73	2.10	±0.08	0.13	2.64	±0.05
D_{32}	.42	2.56	±.16	.04	3.28	±.12
$D_{v0.75}$	.85	.91	±.05	.50	1.75	±.12
D_{31}	.24	2.93	±.25	no acceptable point		

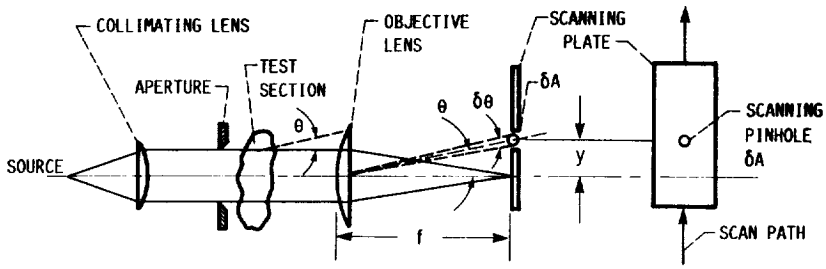

FIGURE 1. - OPTICAL SYSTEM WITH SCANNING PINHOLE.

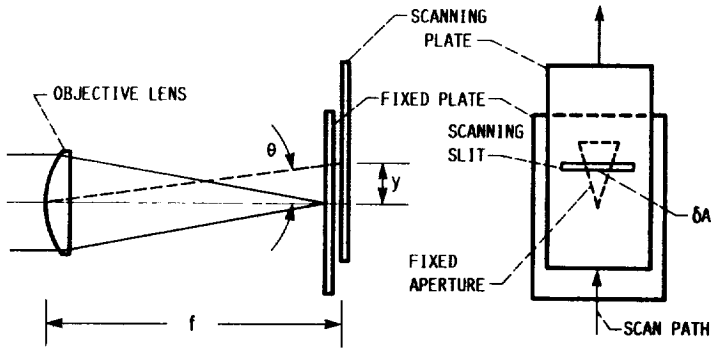

FIGURE 2. - OPTICAL SYSTEM WITH SCANNING SLIT AND FIXED APERTURE.

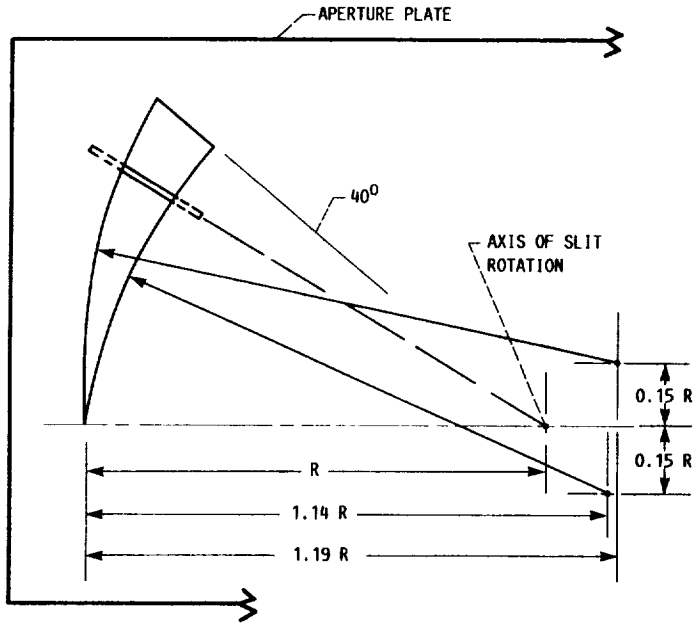

FIGURE 3. - FIXED APERTURE FOR USE WITH SCANNING SLIT.

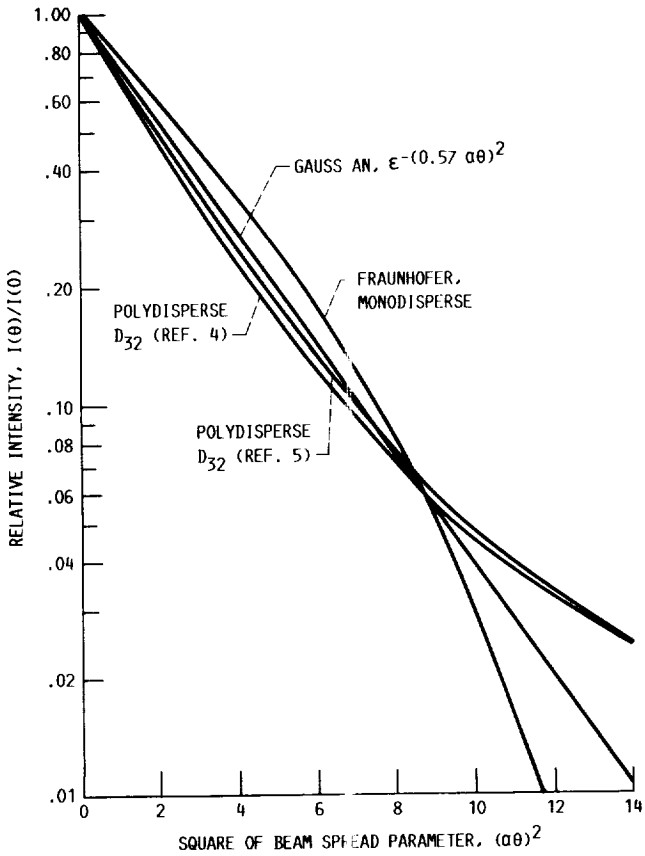

FIGURE 4. - DISTRIBUTION OF FORWARD-SCATTERED LIGHT. (RAY DEVIATION ANGLE θ IN RADIANS.)

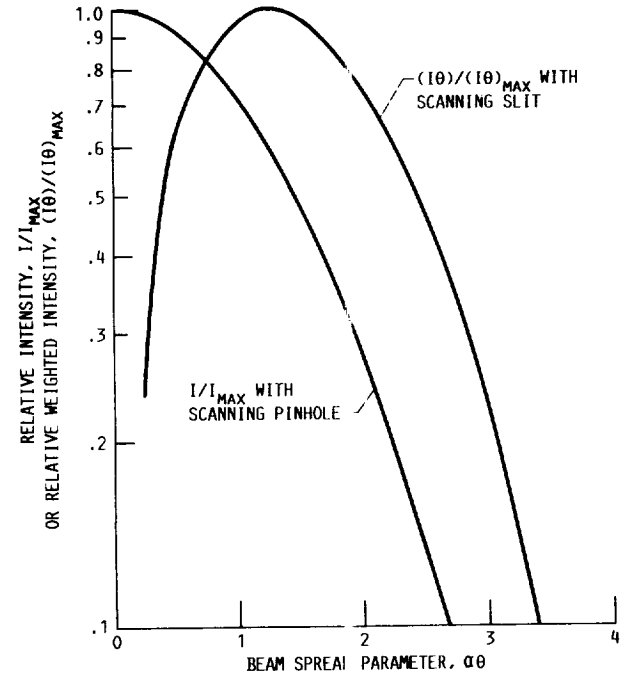

FIGURE 5. - GAUSSIAN DISTRIBUTION OF FORWARD-SCATTERED LIGHT. (RAY DEVIATION ANGLES IN RADIANS.)

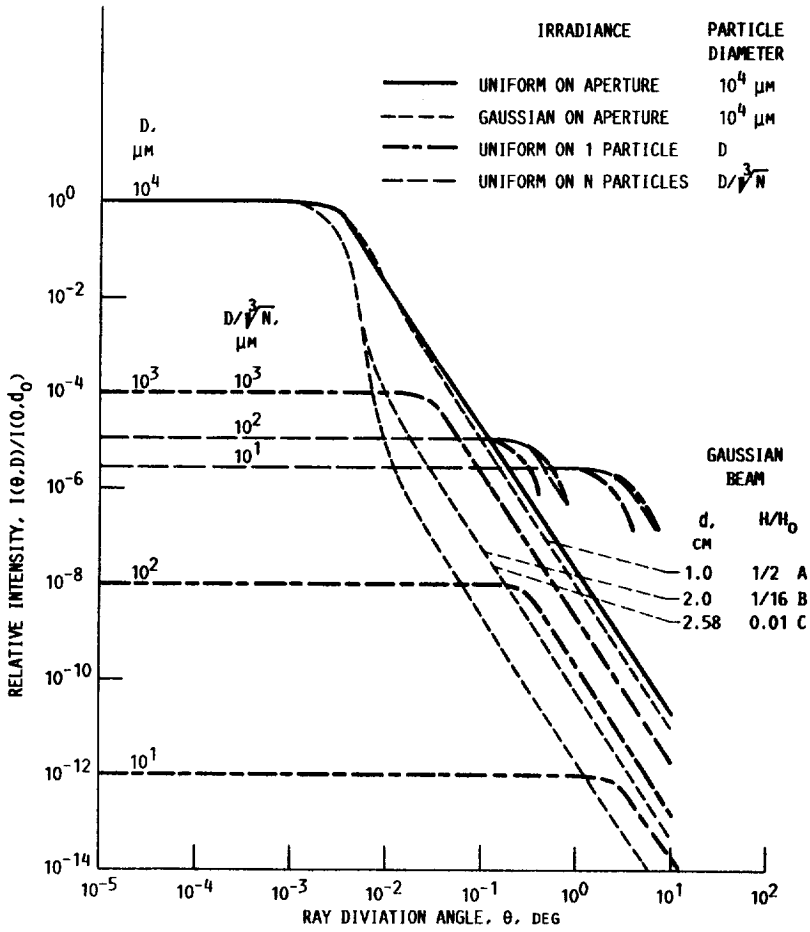

FIGURE 6. - ENVELOPE OF RELATIVE-INTENSITY PEAKS OF FRAUNHOFER DIFFRACTION. WAVELENGTH OF RADIATION, λ, 1 μM: PARTICLE DIAMETER, D; $d_0 = 10^4$ μM.

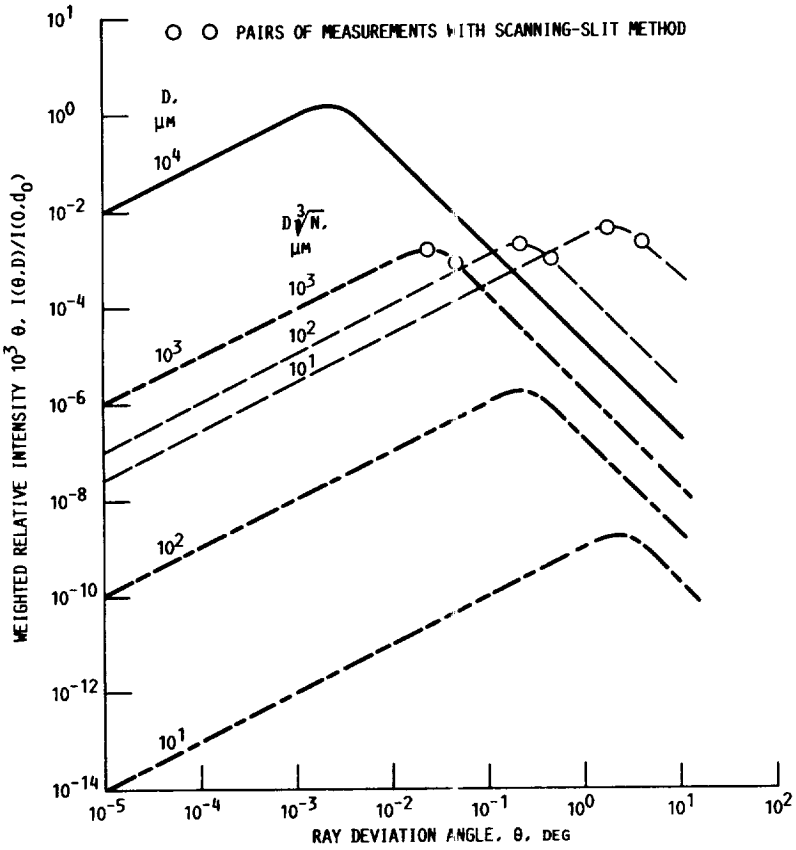

FIGURE 7. - ENVELOPE OF RELATIVE WEIGHTED-INTENSITY PEAKS OF FRAUNHOFER DIFFRACTION. WAVELENGTH OF RADIATION, λ, 1 μm: PARTICLE DIAMETER, D; $d_0 = 10^4$ μm.

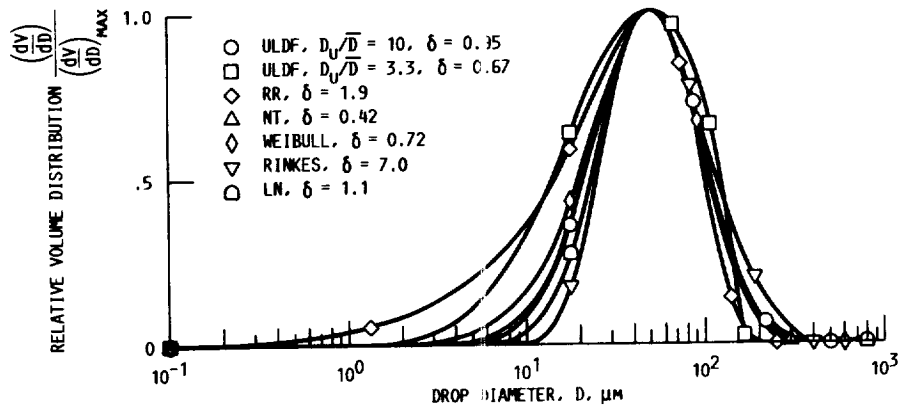

FIGURE 8. - VOLUME DISTRIBUTION OF SIX FUNCTIONS WITH PEAK AMPLITUDE $\overline{D}$ = 50 μm, DISPERSION Δ_V = 1.35.

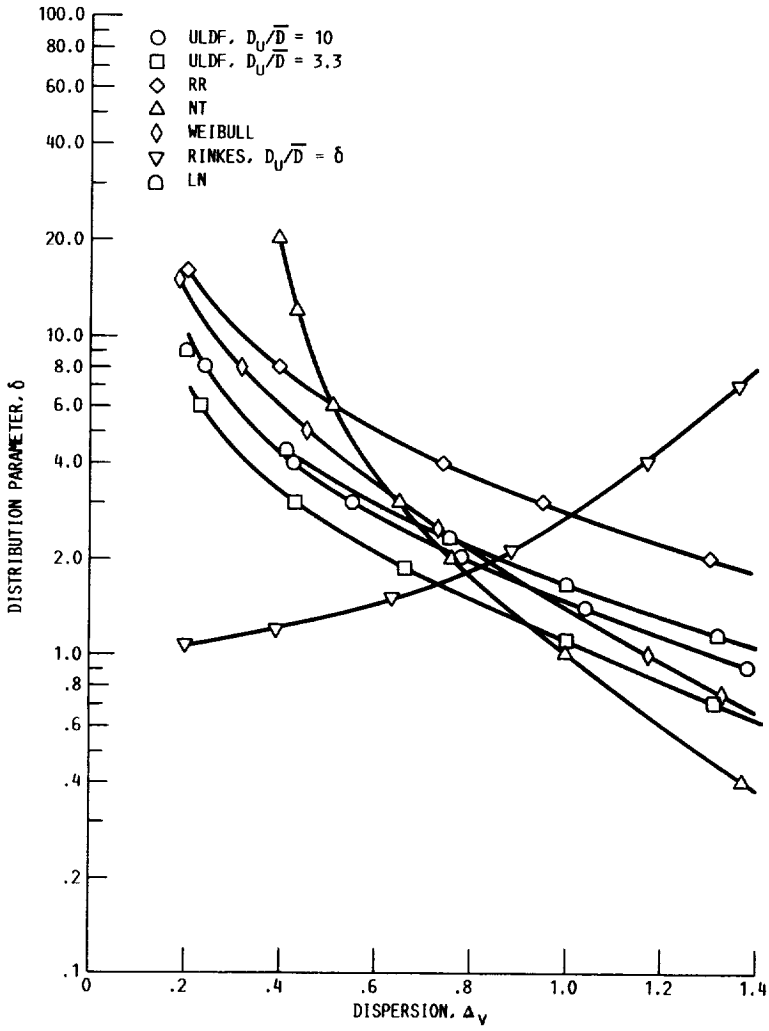

FIGURE 9. - DISTRIBUTION PARAMETER FOR SEVEN DISTRIBUTIONS.

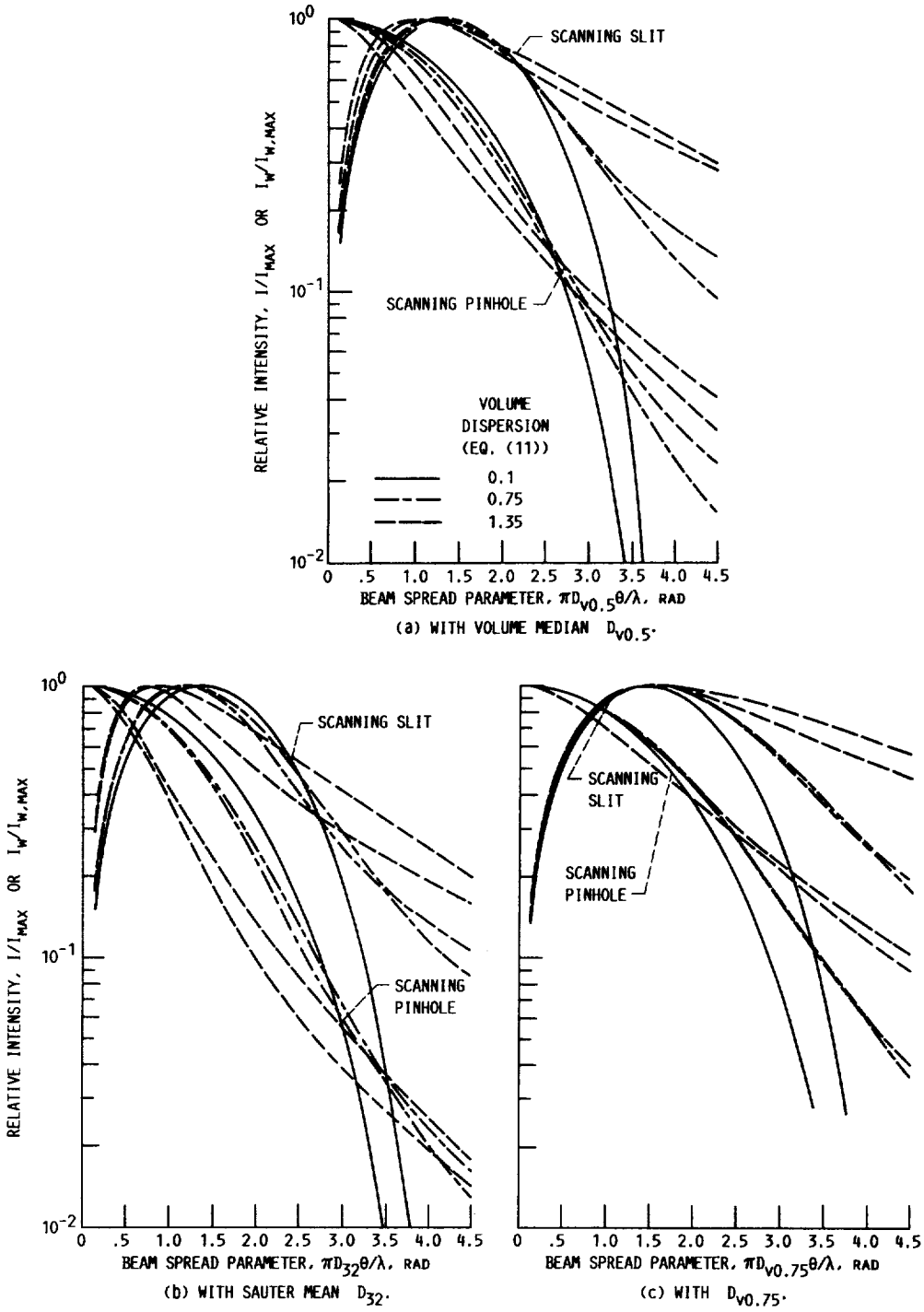

(a) WITH VOLUME MEDIAN $D_{v0.5}$.

(b) WITH SAUTER MEAN D_{32}.

(c) WITH $D_{v0.75}$.

FIGURE 12. - ENVELOPES OF SCATTERED-LIGHT DISTRIBUTION FOR SIX DISTRIBUTION FUNCTIONS AND FOR THREE VALUES OF VOLUME DISPERSION.

PRECEDING PAGE BLANK NOT FILMED

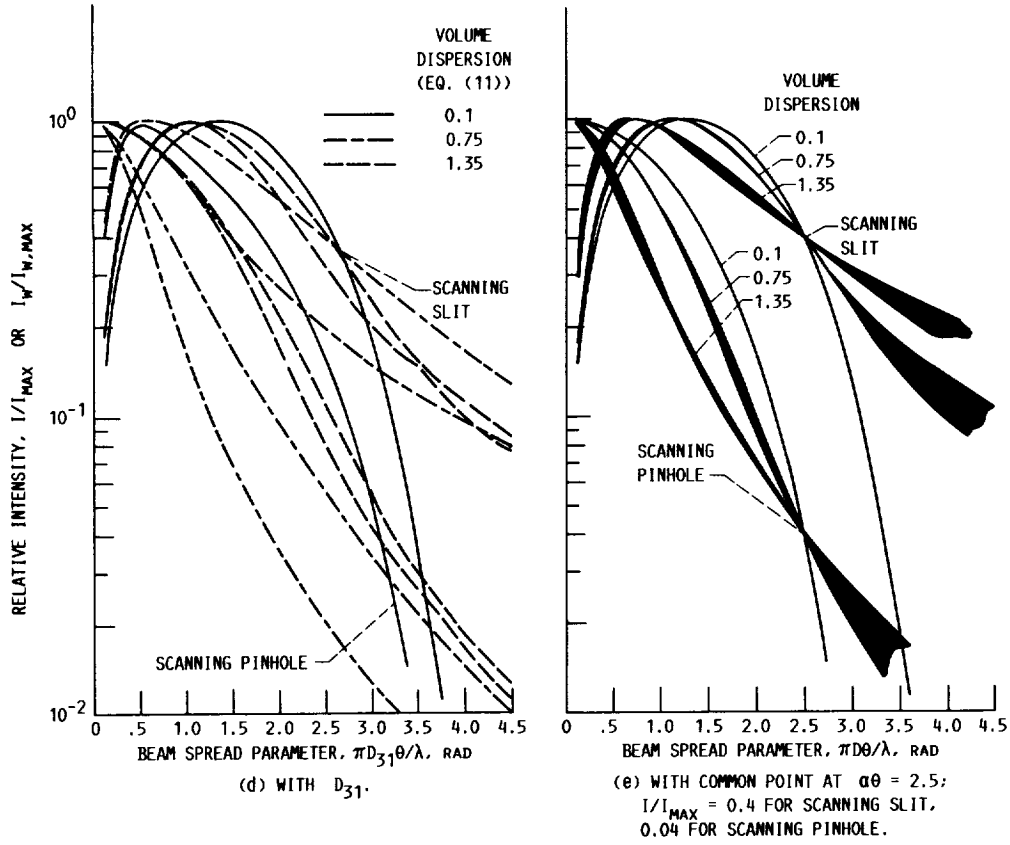

(d) WITH D_{31}.

(e) WITH COMMON POINT AT $\alpha\theta = 2.5$; $I/I_{MAX} = 0.4$ FOR SCANNING SLIT, 0.04 FOR SCANNING PINHOLE.

FIGURE 12. - CONCLUDED.

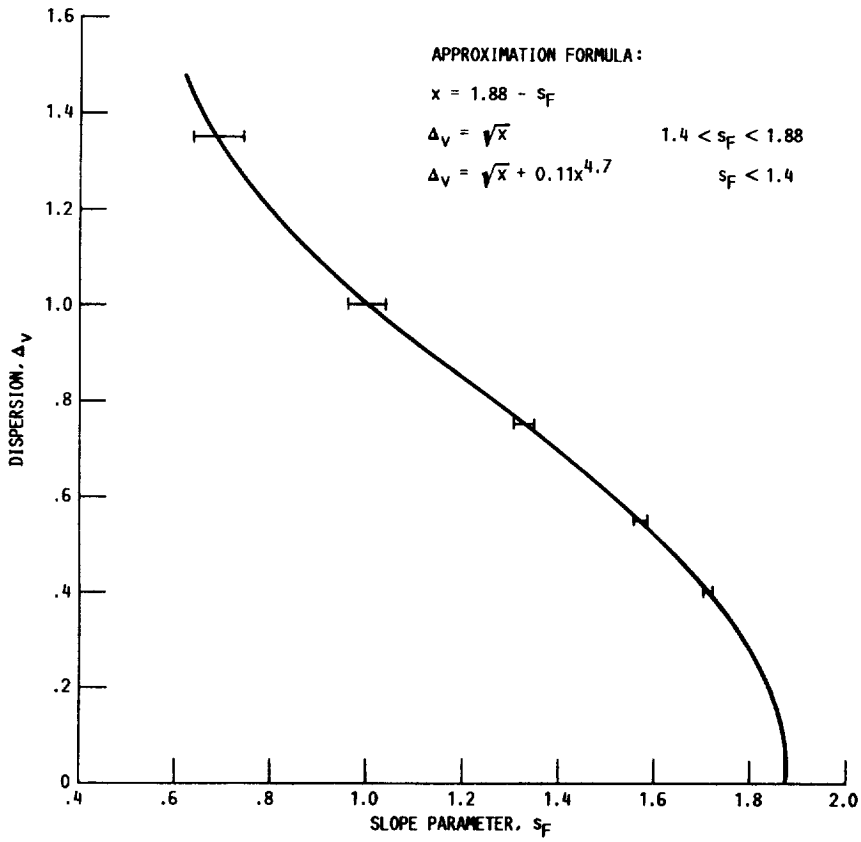

FIGURE 13. - CORRELATION BETWEEN VOLUME DISPERSION AND SLOPE PARAMETER FOR ALL DISTRIBUTION FUNCTIONS.

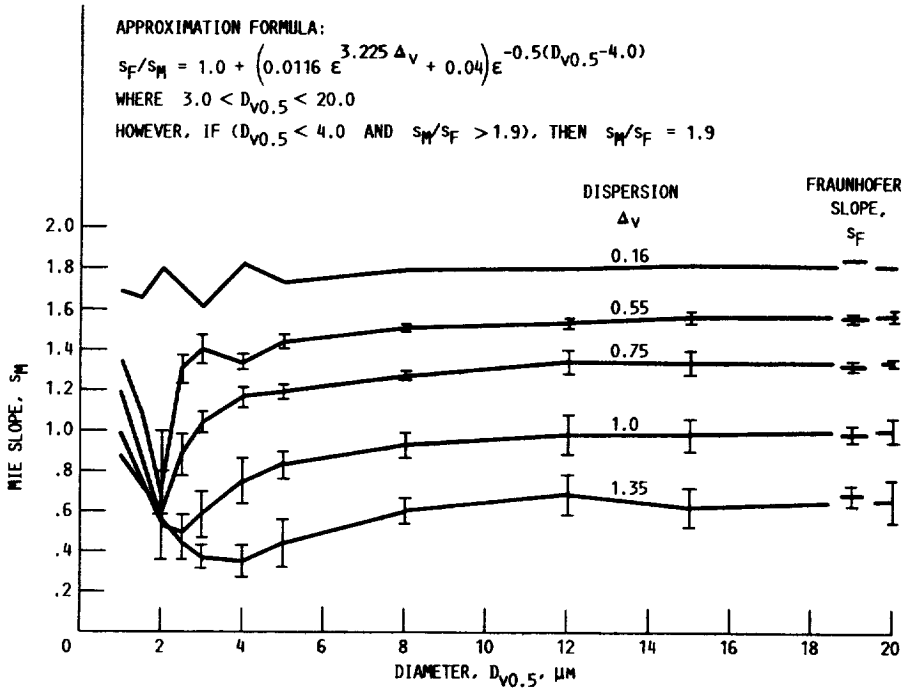

FIGURE 14. - SLOPE OF BEAM SPREAD CURVE FOR MIE SCATTER WITH WATER.

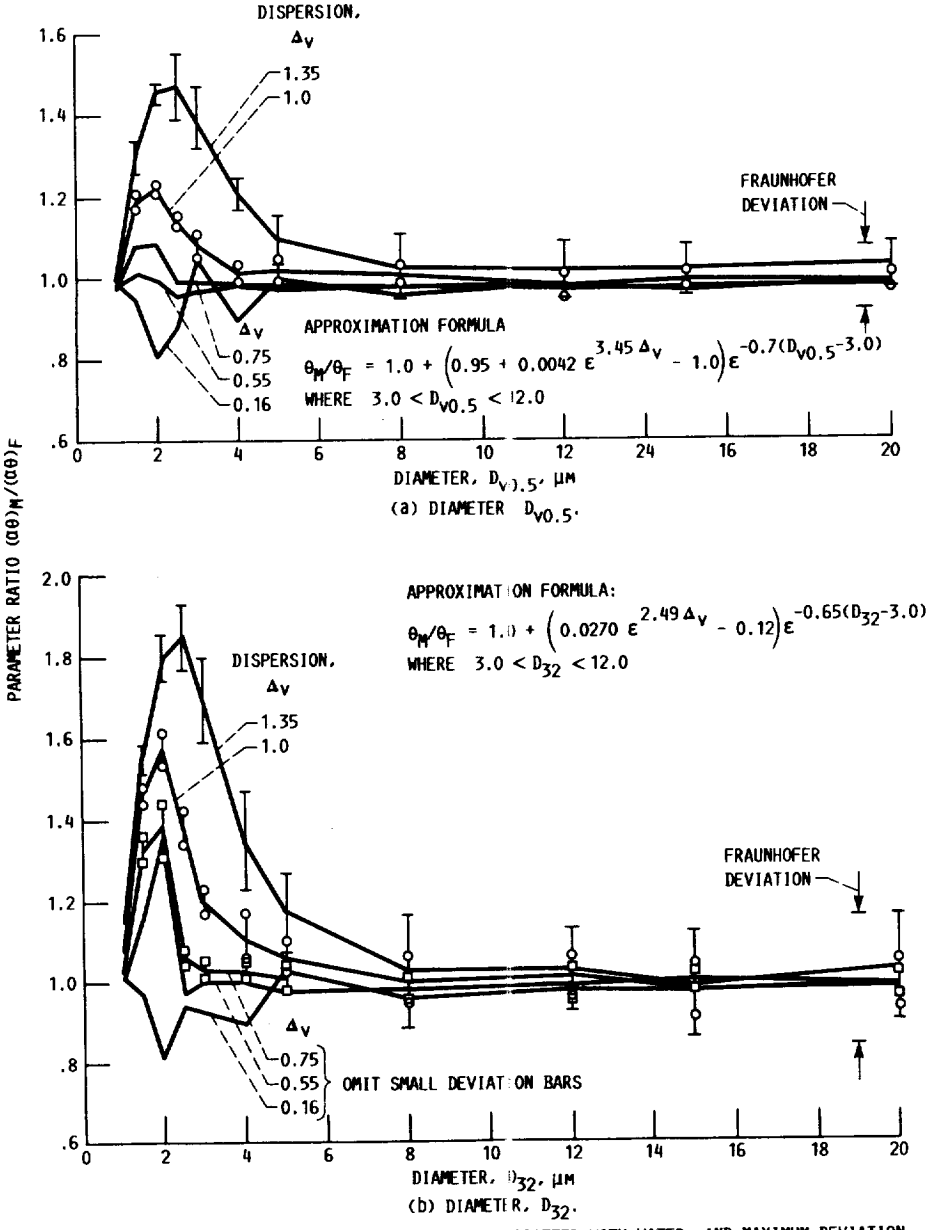

FIGURE 15. - AVERAGE PARAMETER RATIO FOR MIE SCATTER WITH WATER, AND MAXIMUM DEVIATION WITH SEVEN VOLUME DISTRIBUTIONS.

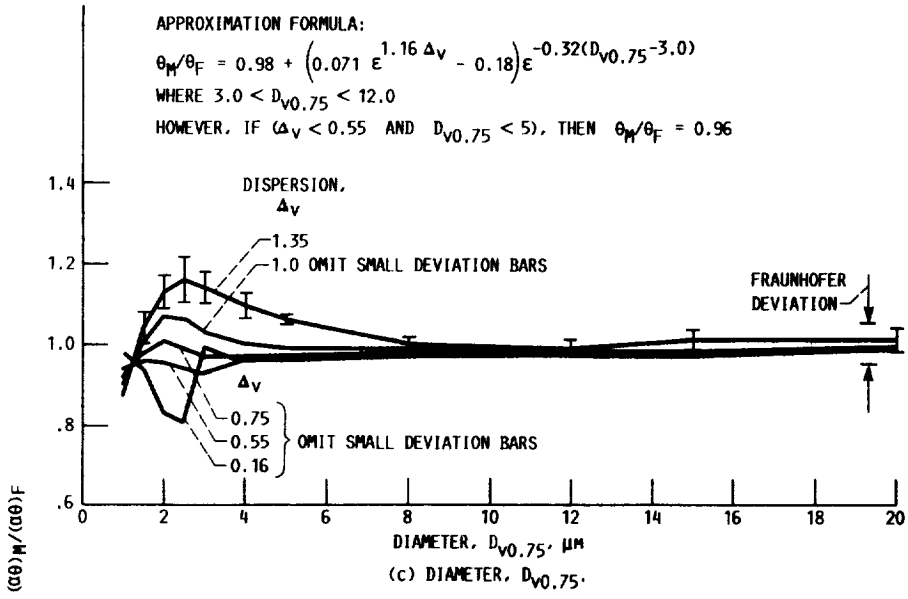

(c) DIAMETER, $D_{V0.75}$.

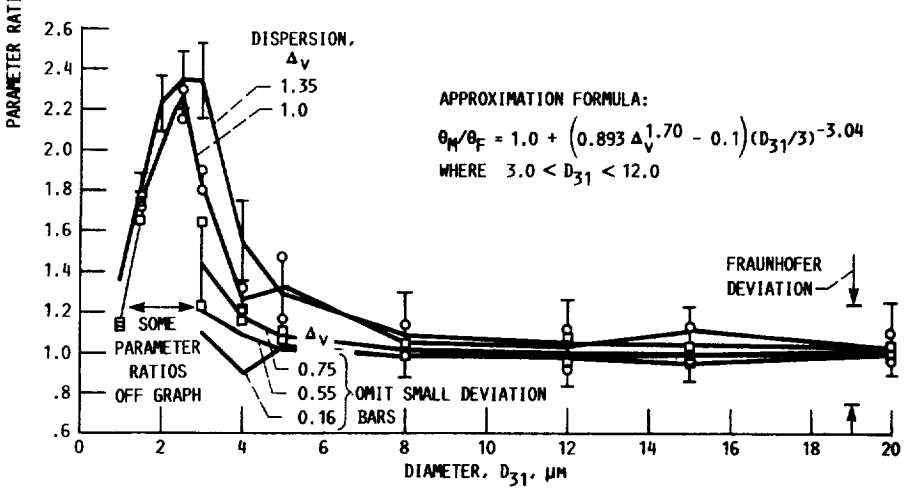

(d) DIAMETER, D_{31}.

FIGURE 15. - CONCLUDED.

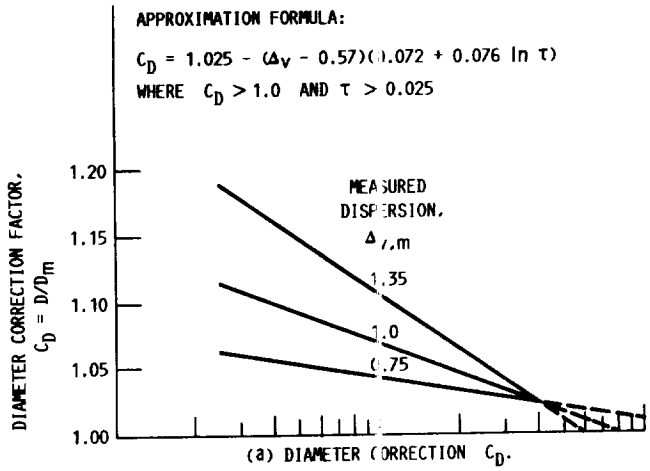

(a) DIAMETER CORRECTION C_D.

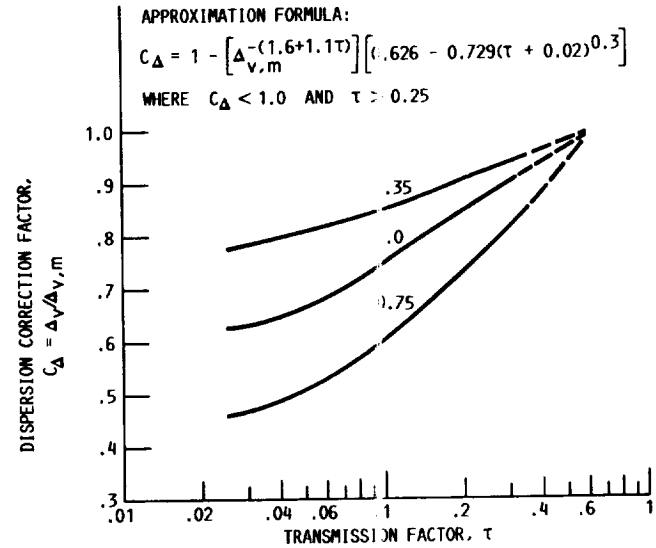

(b) DISPERSION CORRECTION C_Δ.

FIGURE 16. - CORRECTION FACTOR FOR MULTIPLE SCATTER.

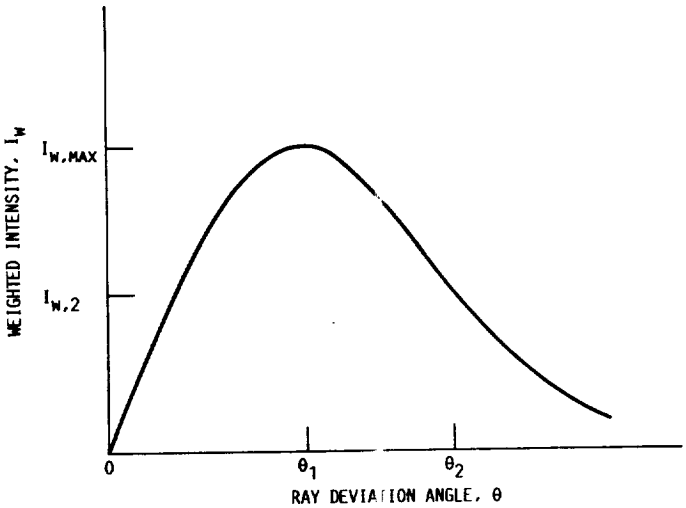

FIGURE 17. - TWO-ANGLE MEASUREMENT WITH SCANNING SLIT.

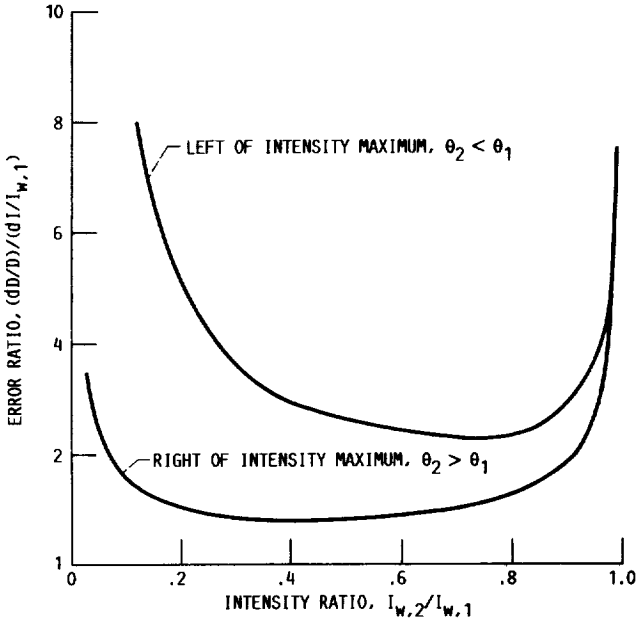

FIGURE 18. - ERROR RATIO, EQUATION (19).

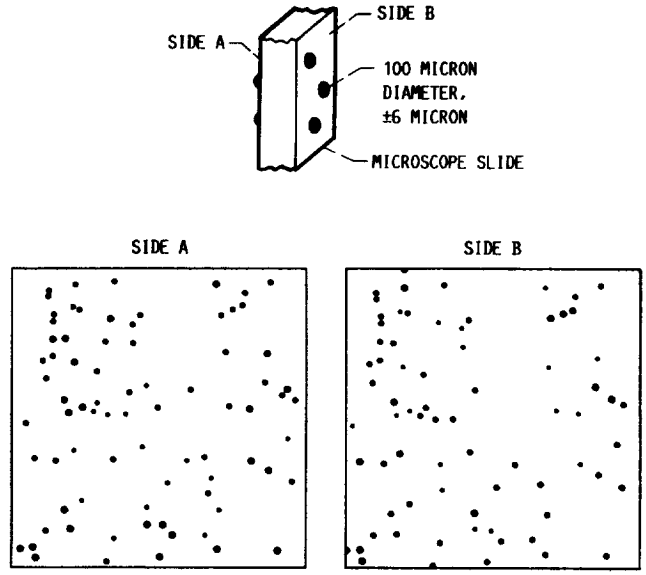

FIGURE 19. - MICROSPHERE CALIBRATION PLATE.

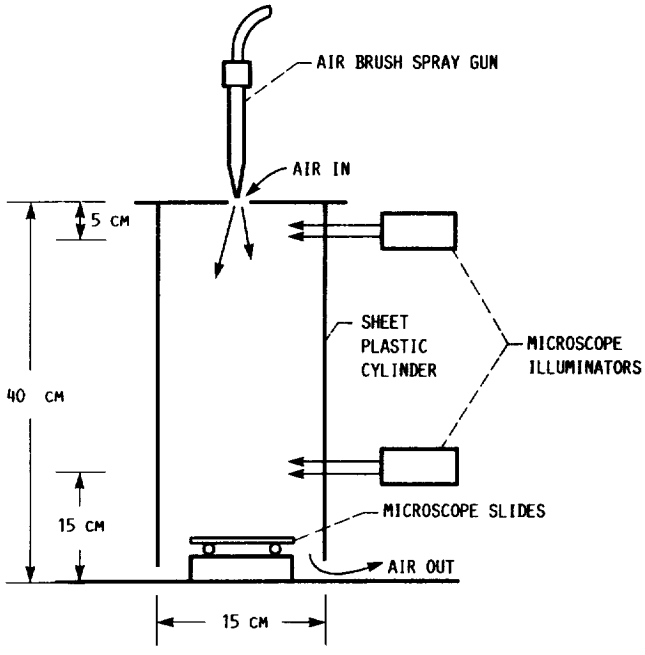

FIGURE 20. - SPRAY CHAMBER FOR MICROSPHERE DEPOSIT ON MICROSCOPE SLIDE.

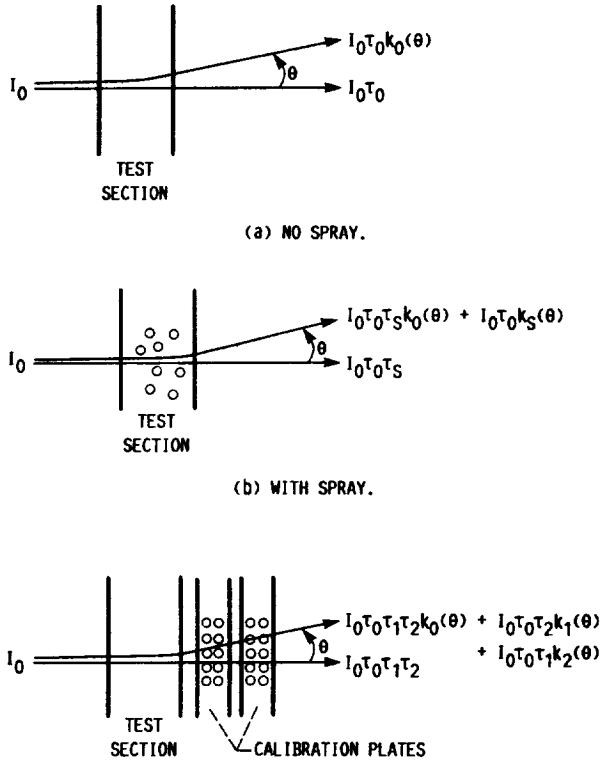

FIGURE 21. - INTENSITY COMPONENTS TRANSMITTED BY TEST SECTION.

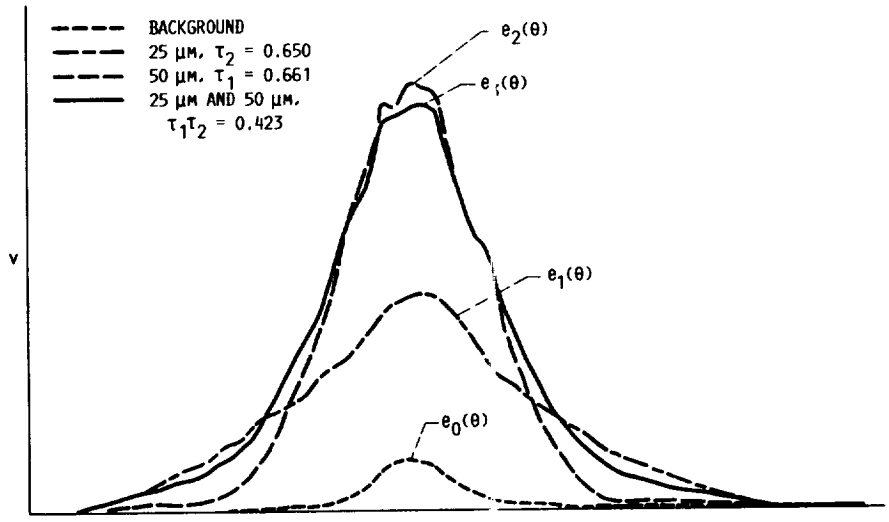

(a) MEASURED DISTRIBUTIONS.

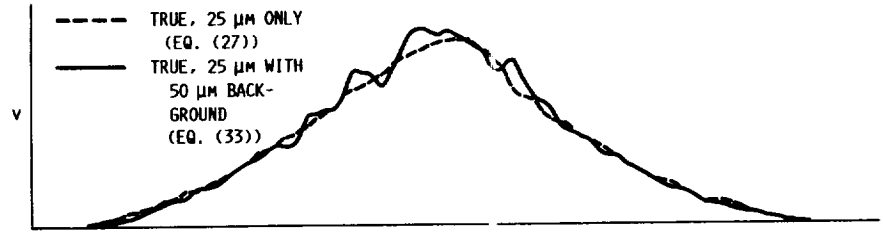

(b) PLATE WITH 25 μm PARTICLES.

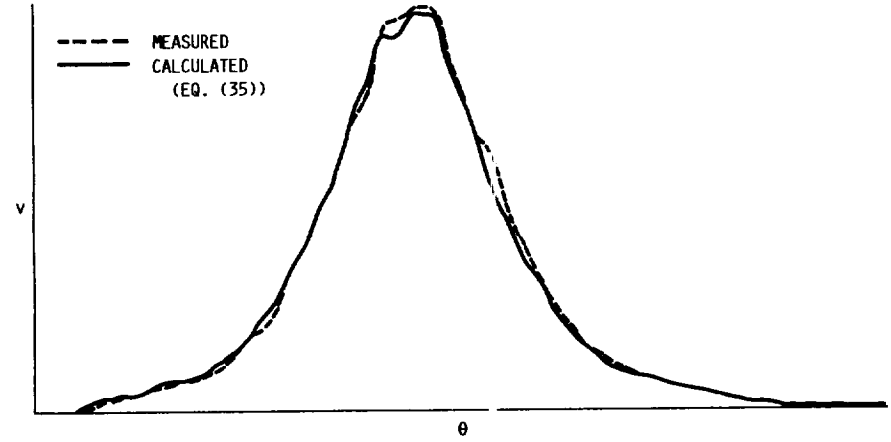

(c) PLATES WITH 25 μm AND 50 μm PARTICLES.

FIGURE 22. - TEST OF CORRECTION FOR BACKGROUND LIGHT WITH CALUBRATION PLATES IN TEST SECTION.

NASA
National Aeronautics and Space Administration

Report Documentation Page

1. Report No.	2. Government Accession No.	3. Recipient's Catalog No.
NASA TM-100968		

4. Title and Subtitle	5. Report Date
Particle Sizing by Weighted Measurements of Scattered Light	October 1988
	6. Performing Organization Code

7. Author(s)	8. Performing Organization Report No.
Donald R. Buchele	E-4396
	10. Work Unit No.
	505-62-01

9. Performing Organization Name and Address	11. Contract or Grant No.
National Aeronautics and Space Administration Lewis Research Center Cleveland, Ohio 44135-3191	
	13. Type of Report and Period Covered
	Technical Memorandum

12. Sponsoring Agency Name and Address	14. Sponsoring Agency Code
National Aeronautics and Space Administration Washington, D.C. 20546-0001	

15. Supplementary Notes

Donald R. Buchele, Distinguished Research Associate.

16. Abstract

A description is given of a measurement method, applicable to a poly-dispersion of particles, in which the intensity of scattered light at any angle is weighted by a factor proportional to that angle. Determination is then made of four angles at which the weighted intensity is four fractions of the maximum intensity. These yield four characteristic diameters: the diameters of the volume/area mean (D_{32} the Sauter mean) and the volume/diameter mean (D_{31}); the diameters at cumulative volume fractions of 0.5 ($D_{v0.5}$ the volume median) and 0.75 ($D_{v0.75}$). They also yield the volume dispersion of diameters. Mie scatter computations show that an average diameter less than three micrometers cannot be accurately measured. The results are relatively insensitive to extraneous background light and to the nature of the diameter distribution. Also described is an experimental method of verifying the conclusions by using two microscope slides coated with polystyrene microspheres to simulate the particles and the background.

17. Key Words (Suggested by Author(s))	18. Distribution Statement
Particle sizing Scattered light Sprays Drop sizing	Unclassified – Unlimited Subject Category 35

19. Security Classif. (of this report)	20. Security Classif. (of this page)	21. No of pages	22. Price*
Unclassified	Unclassified	40	A03

NASA FORM 1626 OCT 86

*For sale by the National Technical Information Service, Springfield, Virginia 22161